Investigating Vulnerable Atheroma Using Combined ^{18}F-FDG PET/CT Angiography of Carotid Plaque with Immunohistochemical Validation

Leon J. Menezes[1], Carl W. Kotze[2], Obi Agu[3], Toby Richards[3], Jocelyn Brookes[4], Vicky J. Goh[5], Manuel Rodriguez-Justo[6], Raymondo Endozo[1], Richard Harvey[2], Syed W. Yusuf[2], Peter J. Ell[1], and Ashley M. Groves[1]

[1]Institute of Nuclear Medicine, University College London, London, United Kingdom; [2]Department of Vascular Surgery, Brighton and Sussex University Hospitals, Brighton, United Kingdom; [3]Department of Vascular Surgery, University College London, London, United Kingdom; [4]Department of Imaging, University College London, London, United Kingdom; [5]Imaging Sciences, King's College London, London, United Kingdom; and [6]Department of Histopathology, University College London, London, United Kingdom

Inflammation and angiogenesis are hypothesized to be important factors contributing to plaque vulnerability, whereas calcification is suggested to confer stability. To investigate this in vivo, we combined CT angiography and PET and compared the findings with immunohistochemistry for patients undergoing carotid endarterectomy. **Methods:** Twenty-one consecutive patients (18 men, 3 women; mean age ± SD, 68.3 ± 7.3) undergoing carotid endarterectomy were recruited for combined carotid ^{18}F-FDG PET/CT angiography. Plaque ^{18}F-FDG uptake was quantified with maximum standardized uptake value, and CT angiography quantified percentage plaque composition (calcium and lipid). Surgical specimens underwent ex vivo CT aiding image registration, followed by immunohistochemical staining for CD68 (macrophage density) and vascular endothelial growth factor (angiogenesis). Relationships between imaging and immunohistochemistry were assessed with Spearman rank correlation and multivariable regression. **Results:** The mean (±SD) surgically excised carotid plaque ^{18}F-FDG metabolism was 2.4 (±0.5) versus 2.2 (±0.3) contralaterally ($P = 0.027$). There were positive correlations between plaque ^{18}F-FDG metabolism and immunohistochemistry with CD68 ($\rho = 0.55$; $P = 0.011$) and vascular endothelial growth factor ($\rho = 0.47$; $P = 0.031$). There was an inverse relationship between plaque ^{18}F-FDG metabolism and plaque percentage calcium composition on CT ($\rho = -0.51$; $P = 0.018$) and between calcium composition and immunohistochemistry with CD68 ($\rho = -0.57$; $P = 0.007$). Regression showed that maximum standardized uptake value and calcium composition were independently significant predictors of angiogenesis, and calcium composition was a predictor of macrophage density. **Conclusion:** We provide in vivo evidence that increased plaque metabolism is associated with increased biomarkers of angiogenesis and inflammation, whereas plaque calcification is inversely related to PET and histologic biomarkers of inflammation.

Key Words: carotid atherosclerosis; computed tomography angiography; ^{18}F-FDG positron emission tomography

J Nucl Med 2011; 52:1698–1703
DOI: 10.2967/jnumed.111.093724

The identification of atheroma at risk of causing cardiovascular events has been investigated for many years (*1*). The role of imaging in this respect has been 2-fold: first, to anatomically characterize atheroma with features of vulnerability, and second, to investigate key components of plaque pathogenesis such as inflammation and angiogenesis (*2*). PET (*3,4*) and dynamic MRI (*5*) have been used to image the latter, whereas high-resolution MRI (*6*) and CT (*7,8*) have been used to characterize plaque morphology. CT is particularly of interest because this is an ideal imaging modality for coronary arteries, and there is evidence that calcium composition predicts the likelihood of acute coronary syndromes (*9*).

To synergistically image plaque vulnerability, it may be desirable to use a multimodality approach so that anatomy and pathophysiology may be assessed together. The value of such an approach has been shown in oncology (*10*) and cardiology (*11*). Indeed, this combined approach has now been applied to carotid plaque imaging (*12,13*). However, the findings have been conflicting with respect to the relationship between uptake on PET and anatomic imaging: lipid-rich necrotic core plaques demonstrated higher ^{18}F-FDG uptake than calcified or collagen plaques in one study (*12*), but no strong correlations between ^{18}F-FDG uptake and the CT- or MRI-assessed composition of the plaques existed in another (*13*). Moreover, gold standard histologic comparison was unavailable for either of these studies. Histologic comparison may provide important insight into atheroma pathogenesis.

Therefore, in this study, we combined carotid plaque ^{18}F-FDG PET/CT with carotid CT angiography in patients undergoing carotid endarterectomy and performed bioassays of macrophage density (CD68; Dako) and angiogenesis (vascu-

Received May 25, 2011; revision accepted Aug. 17, 2011.
For correspondence or reprints contact: Ashley M. Groves, Institute of Nuclear Medicine, University College London, 5th Floor, University College Hospital, 235 Euston Rd., London NW1 2BU, U.K.
E-mail: drashleygroves@hotmail.com.
Published online Oct. 11, 2011.
COPYRIGHT © 2011 by the Society of Nuclear Medicine, Inc.

lar endothelial growth factor [VEGF]; Dako) in the resected specimens.

MATERIALS AND METHODS

After approval from the institutional ethics committee, 21 consecutive patients (18 men, 3 women; mean age ± SD, 68.3 ± 7.3 y) undergoing carotid endarterectomy were recruited for combined carotid ^{18}F-FDG PET/CT angiography. All patients had 70% or greater carotid stenosis as determined by duplex ultrasound. All patients gave informed consent. The patients' clinical characteristics are shown in Supplemental Table 1 (available online only at http://jnm.snmjournals.org).

Image Acquisition

^{18}F-FDG PET/CT. After a 6-h fast, patients received an intravenous injection of 190 MBq of ^{18}F-FDG. The mean ^{18}F-FDG uptake time was 92.4 ± 4.6 min (*14*). Using a Discovery LS PET/CT scanner (GE Healthcare), we imaged a single bed position (148.75 mm) centered on the carotid bifurcation, with the patients supine with their arms positioned beside their torso. CT for attenuation correction was performed: 140 kVp and 80 mAs; tube rotation time, 0.8 s; detectors, 64 × 0.625 mm; pitch, 1.5; and collimation, 5 mm. Maintaining patient position, we obtained a PET scan covering an area identical to that covered by CT. All images were acquired in 2-dimensional mode, consisting of an emission scan of 10 min. PET images were reconstructed with CT for attenuation correction using CT maps. Transaxial emission images of 3.9 × 3.9 × 4.25 mm (in-plane matrix size, 128 × 128) were reconstructed using ordered-subsets expectation maximization with 2 iterations and 28 subsets. The *z*-axis coverage was 148.75 mm, resulting in 35 slices.

CT Carotid Angiography. Immediately after PET, CT carotid angiography was performed from the aortic arch to the base of skull, using 50 mL of intravenous contrast medium (Omnipaque 350 [GE Healthcare]; 5 mL/s), followed by 50 mL of normal saline, with the patient maintained in the same position. Scanning parameters were 120 kVp; 150 mAs; tube rotation time, 0.5 s; detectors, 64 × 0.625 mm; pitch, 0.984; and collimation, 2.5 mm. The field of view was 250 × 250 mm, and matrix size was 512 × 512. CT images were reconstructed with a 0.625-mm slice thickness and no interval.

Image Analysis

All images were analyzed using the carotid bifurcation as an anatomic landmark to allow direct comparison of histology with ^{18}F-FDG PET/CT and CT angiography.

^{18}F-FDG PET/CT. Images were reported in consensus by a dual-accredited nuclear medicine physician–radiologist with a cardiovascular interest (>5 y experience, with >4 y experience at quantifying carotid plaque ^{18}F-FDG uptake) and a radiologist with a cardiovascular and PET special interest (>4 y experience at quantifying carotid plaque ^{18}F-FDG uptake). Images were loaded on an Advantage Workstation (GE Healthcare). Regions of interest were drawn on the carotid artery wall at the bifurcation, and the maximum standardized uptake value (SUV_{max}) was recorded. The SUV_{max} was normalized to the blood-pool SUV_{max} value measured from the internal jugular vein, giving the tissue-to-background ratio.

CT Angiography. One investigator, a radiologic technologist with more than 10 y of experience in CT angiography, unaware of the PET/CT findings, evaluated the CT angiograms of the surgical side. Images were loaded onto an Advantage Workstation. Colorimetric analysis of the carotid bifurcation was used to quantify different plaque components. Different Hounsfield unit (HU) ranges were considered to represent different plaque components: calcification, greater than 600 HUs, and lipids, 20–60 HUs (*7,8*). Figures 1B and 2B show examples of the colorimetric analysis drawn on the CT images. The software calculated the percentage plaque composition with lipids and calcification. To determine the variability of the plaque composition measurement, the images were reanalyzed by the same observer, 3 mo apart in a masked manner. The intraclass correlation coefficients were 0.996 (95% confidence interval, 0.989–0.999) for percentage calcification and 0.965 (95% confidence interval, 0.901–0.988) for percentage lipids.

Image Registration. The PET and CT angiography images were automatically coregistered by the Advantage Workstation (Figs. 1A and 2B).

Histologic Preparation and Analysis. All patients were operated on within 2 wk of imaging. The endarterectomy specimens were fixed in 10% formalin. To maximize in vivo registration with histologic sections, the resected endarterectomy specimens underwent ex vivo CT examination before sectioning (Figs. 1C and 2C). Using the carotid bifurcation as the anatomic landmark, the radiologist and histopathologist in consensus carefully coregistered the endarterectomy specimens to the carotid plaque images (in vivo CT, CT angiography, and ex vivo CT images). In all patients, histologic analyses were performed at the carotid bifurcation for direct comparison of PET and CT angiography.

Histologic sections (4 μm thick) from each tissue block in each patient were stained with hematoxylin and eosin and monoclonal

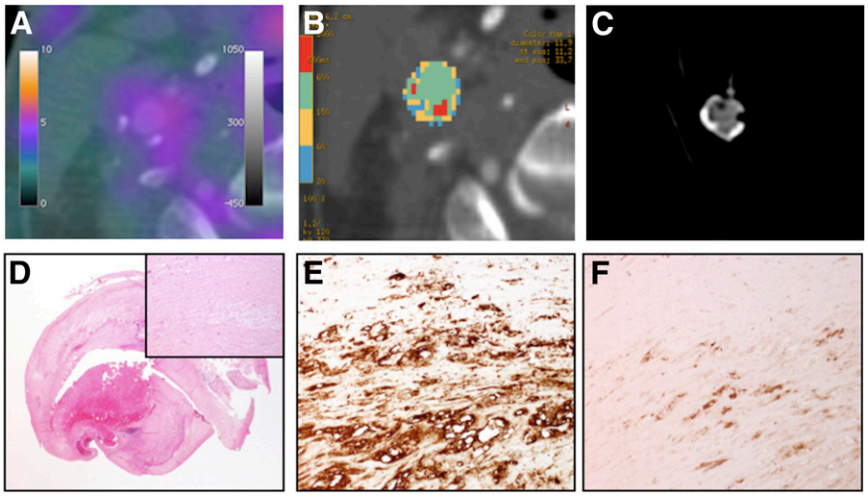

FIGURE 1. (A) Contrast-enhanced PET/CT scan showing carotid bifurcation with increased ^{18}F-FDG uptake (scale bar on left, SUVmax; scale bar on right, CT window level and width). (B) Colorimetric analysis of plaque component areas on CT scan. Ranges of HU values represent different plaque components: azure, lipid core (20–60 HU), and red, calcification (600–2,000 HU). (C) Axial CT scan of ex vivo carotid artery specimen. (D) Hematoxylin and eosin low-power magnification (×12.5) and detail magnification (×200) of same carotid bifurcation. (E) CD68-stained (×200) section of carotid bifurcation. (F) VEGF-stained (×200) section of carotid bifurcation.

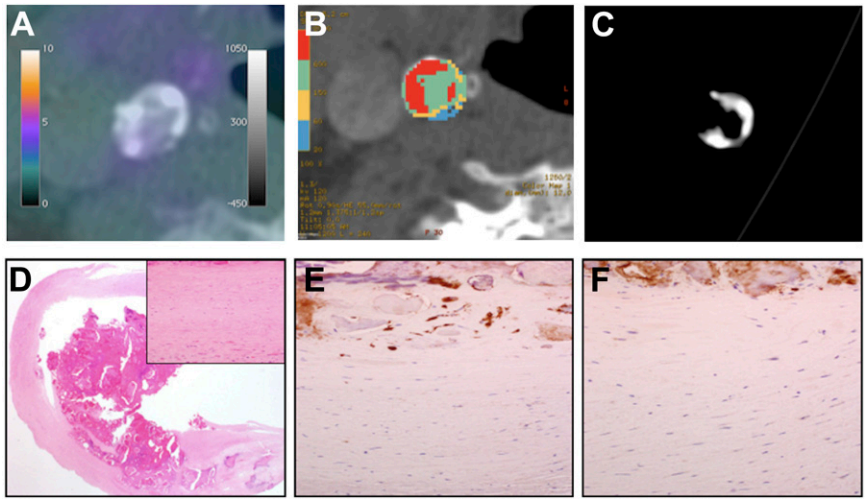

FIGURE 2. (A) Contrast-enhanced PET/CT scan showing carotid bifurcation with low ^{18}F-FDG uptake (scale bar on left, SUVmax; scale bar on right, CT window level and width). (B) Colorimetric analysis of plaque component areas on CT. Ranges of HU values represent different plaque components: azure, lipid core (20–60 HU), and red, calcification (600–2,000 HU). (C) Axial CT scan of ex vivo carotid artery specimen. (D) Hematoxylin and eosin low-power magnification (×12.5) and detail magnification (×200) of same carotid bifurcation. (E) CD68-stained (×200) section of carotid bifurcation. (F) VEGF-stained (×200) section of carotid bifurcation.

antibodies CD68 (dilution, 1/50) for macrophages (*3*) and VEGF (dilution, 1/100) for angiogenesis (*15*). Immunohistochemical staining of tissue sections was performed on the fully automated BondmaX system (Leica Microsystems) and was used in conjunction with the Bond Polymer Refine system. All sections were stained at the same time.

Automated image quantification was performed using digital microscopy to analyze the immunohistochemical staining. All the slides were scanned using Mirax Scan (Carl Zeiss), and the images provided by the software were exhibited on a liquid crystal display monitor under contrast, focus, saturation, and white balance standardization. To evaluate the staining intensity, an image analysis system (HistoQuant; 3DHistech) was used. The software identified the immunohistochemical staining to be quantified by minimizing background-staining artifacts using image filters. Because the software recognized the positive nuclei staining of all different intensities, the quantification was processed in each tissue microarray section (spot) automatically by the software. Each spot's numeric data of staining intensity average was exported to a Microsoft Excel file.

CD68-stained macrophages were expressed as a percentage of plaque area. In cases for which the plaque occupied more than 180° of the vessel wall, the value for percentage plaque CD68 staining in the most inflamed half of the vessel wall was recorded (*4*). VEGF staining of endothelial cells was expressed as a score of number of stained cells and intensity.

Statistical Analysis

A paired *t* test was used to compare the PET findings between the plaque surgically operated on and the contralateral carotid plaque. The intraclass correlation coefficient was used to assess intraobserver variability of CT plaque composition measurements. Spearman correlation coefficients (ρ) were calculated for the association between imaging parameters and immunohistochemistry. To check whether any of the imaging parameters were independently statistically significant, they were introduced in a multiple regression model, and backward stepwise regression analysis was performed. All statistical tests were performed using software from GraphPad (Prism and InStat).

RESULTS

The mean (±SD) surgical carotid plaque ^{18}F-FDG metabolism (SUV_{max}) was 2.4 ± 0.5 versus 2.2 ± 0.3 contralaterally (P = 0.027). There was no significant difference in mean surgical carotid plaque tissue-to-background ratio versus contralaterally (P = 0.264).

Comparison Between ^{18}F-FDG PET and CT Angiographic Findings

The correlation between plaque ^{18}F-FDG metabolism and percentage plaque calcification on CT angiography was −0.51 (P = 0.018) (Fig. 3). The correlation between plaque ^{18}F-FDG metabolism and percentage plaque lipid on CT angiography was 0.13 (P = 0.569).

Comparison of ^{18}F-FDG PET Findings with Histology

The correlation between plaque ^{18}F-FDG metabolism and plaque CD68 expression on immunohistochemistry was 0.55

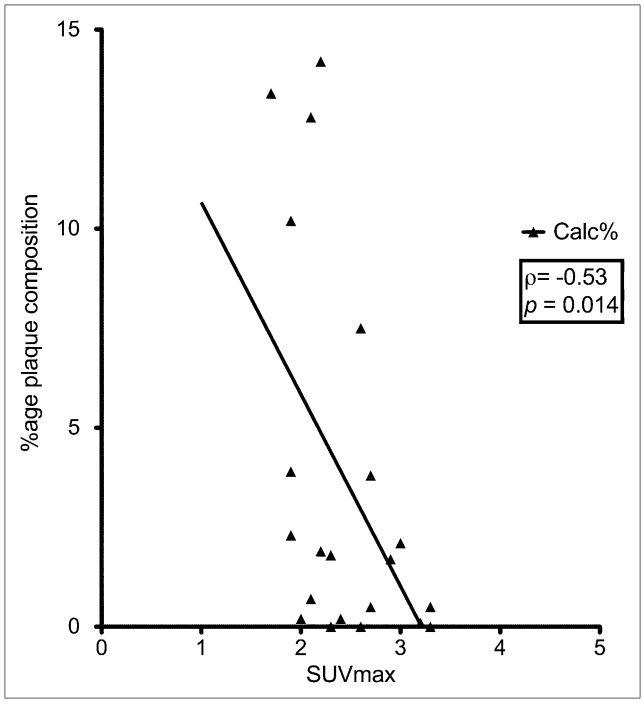

FIGURE 3. Scatterplot to show Spearman rank correlation of SUV_{max} with percentage plaque composition by calcium.

($P = 0.011$) (Fig. 4). The correlation between plaque ^{18}F-FDG metabolism and plaque VEGF expression on immunohistochemistry was 0.47 ($P = 0.03$) for VEGF.

Comparison of CT Angiographic Findings with Histology

The correlation between plaque calcium composition and plaque CD68 expression on immunohistochemistry was -0.57 ($P = 0.007$). The correlation between plaque calcium composition and plaque VEGF expression on immunohistochemistry was -0.03 ($P = 0.902$). The correlation between plaque lipid composition and plaque CD68 expression on immunohistochemistry was -0.04 ($P = 0.853$). The correlation between plaque lipid composition and plaque VEGF expression on immunohistochemistry was -0.06 ($P = 0.790$).

Regression Analysis

When all imaging parameters were introduced into a multivariable regression model and backward stepwise regression was performed, percentage calcification remained statistically significant ($P < 0.05$) for CD68 expression, and SUV_{max} and percentage calcification remained statistically significant ($P < 0.05$) for VEGF expression (Table 1).

DISCUSSION

In this study, morphologic composition on CT with respect to increasing arterial calcification reflected underlying hypometabolism as measured by ^{18}F-FDG PET. Furthermore, plaque calcification was inversely related to a bioassay of macrophages, whereas plaque with high ^{18}F-FDG metabolism was associated with a raised bioassay of macrophages.

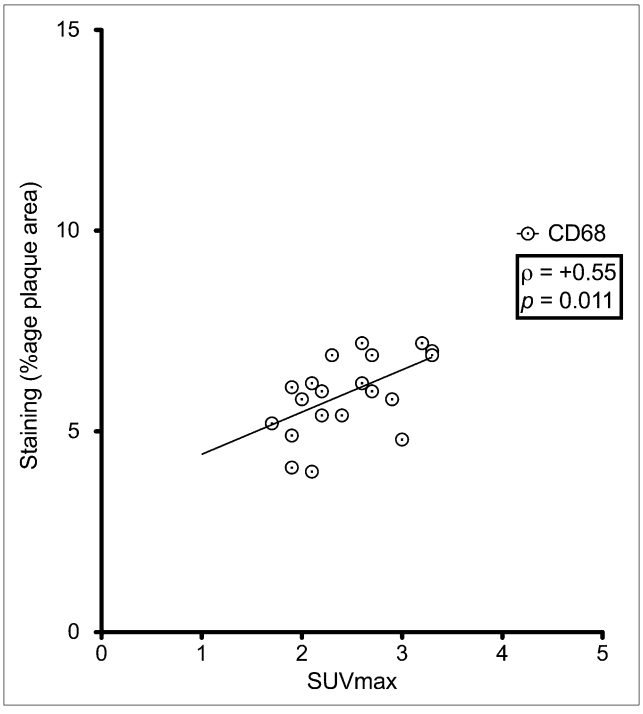

FIGURE 4. Scatterplot to show Spearman rank correlation of SUV_{max} with plaque staining intensity with CD68.

These findings support current evidence that increased ^{18}F-FDG plaque metabolism is associated with instability (*2,3*), whereas increased plaque calcification confers stability (*16*).

Our PET/CT angiography findings showed an inverse relationship between ^{18}F-FDG arterial uptake on PET and arterial calcification. The inverse relationship would help explain why vascular ^{18}F-FDG uptake and calcification rarely overlap (*17,18*). This negative correlation supports the view that calcification represents a late stage of atherosclerosis (*19,20*)—important with respect not only to carotid artery disease but also to coronary artery disease. Coronary arteries are difficult to image using PET because of their size and cardiac motion. In contrast, CT is an ideal coronary artery imaging technique. Potentially, differences in plaque composition on CT angiography may be useful for the noninvasive identification of atherosclerotic plaques associated with higher risk (*9,21*), for which one would expect that plaques with spotty calcification (*16*) would overlap with the plaques we identified with little percentage calcification by composition and inflammation by metabolism. The histologic findings in our study in relation to plaque composition would seem to support this hypothesis. Whether plaque characterization on PET/CT angiography could be translated into medical practice remains to be seen. Currently, risk stratification is based on clinical data. PET/CT angiography may recognize plaques at higher risk, according to their composition and metabolism. However, we await prognostic data from large outcome studies (*22*), and improvements in the imaging technology, as alluded to in the study limitations.

The finding that there is a relationship between morphologic plaque composition and ^{18}F-FDG PET is confirmed by others using MRI, with lipid-rich plaques having more ^{18}F-FDG uptake than either collagen-rich or calcified plaques (*12*). This finding, however, has not been universal, with another group finding no correlation between standardized uptake value and calcification (*13*). Nonetheless, our study findings are supported further by our immunohistochemical analysis, with which we were also able to show inverse relationships between plaque calcium content and the bioassay of plaque inflammation (CD68). CD68 is a marker for macrophage activity and has been shown by histologic studies to be raised in vulnerable carotid plaque (*3,23*). The fact that we found statistically significantly lower levels of CD68 in calcified plaque would support the hypothesis that such plaques may be more stable.

The bioassay findings in relation to ^{18}F-FDG PET are interesting, especially because there has been a paucity of histologically validated carotid PET plaque studies (*2,3,23*). We found that VEGF expression in plaque is related to ^{18}F-FDG uptake. VEGF, an inducer of angiogenesis, may enhance plaque formation and destabilization in vulnerable atherosclerotic plaque (*24*). Indeed, angiogenesis is believed to be a central component in the pathogenesis of unstable atheroma (*2*). It would seem that a variety of cellular components and molecular mechanisms within the endothelial lesion, including macrophage infiltration and angiogenesis,

TABLE 1
Results of Multivariable Linear Regression Analyses, with CD68 and VEGF as Dependent Variables of Interest and Percentage Calcium and SUVmax as Statistically Significant Predictors

Dependent variable	Predictor	B coefficient	95% Confidence interval	*P*
CD68	Percentage calcium	−0.1038	−0.2001 to −0.00743	0.0363
VEGF	Percentage calcium	0.02863	3.0002653–0.05700	0.0481
VEGF	SUV_{max}	0.2670	0.00967–0.5243	0.0428

may contribute to ^{18}F-FDG uptake in inflamed atherosclerotic plaque (*25*).

When performing carotid imaging studies, there are several methodologic considerations of which to be aware. There is a difference regarding the precise methodologic details of arterial imaging with ^{18}F-FDG PET (*26*). Some groups favor SUV_{max} measurements (*27*), others standardized uptake value normalized to blood (target to background ratio) (*3*) or whole-vessel analysis (*14*). SUV_{max} measurements have shown to be the most reproducible ^{18}F-FDG measurements in carotid arteries (*28*). The lack of difference in carotid tissue-to-background ratio between the operated side and nonoperated side may be due to the extra variability introduced by normalizing the uptake. Alternatively, given that the degree of uptake in the nonoperated side was greater than has been described in healthy populations (*19,29*), the lack of difference may reflect the possibility that the pathophysiologic processes behind plaque vulnerability also exert effects throughout the vascular tree, as has been shown in the coronary circulation (*30*).

In our study, we obtained SUV_{max} measurements at the carotid bifurcation to enable precise imaging–histologic correlation. Attention to detail was made to maximize image registration of morphology to histology. Nevertheless, the tissue thickness encompassed by imaging (mm) is different from the tissue thickness covered by immunohistochemistry (μm), and this difference is an inherent limitation of all such published studies (*2–4,27*). All published histologically validated carotid plaque studies have limited-size populations, with heterogeneity in terms of symptoms, time to surgery, and medications (*2–4,31*), reflecting the logistic difficulties of these types of studies.

CONCLUSION

We provide in vivo evidence that increased plaque metabolism is associated with increased biomarkers of angiogenesis and inflammation, whereas plaque calcification is inversely related to PET and histologic biomarkers of inflammation. Whether these findings can be translated into the clinic with respect to risk stratification or treatment monitoring should be addressed.

DISCLOSURE STATEMENT

The costs of publication of this article were defrayed in part by the payment of page charges. Therefore, and solely to indicate this fact, this article is hereby marked "advertisement" in accordance with 18 USC section 1734.

ACKNOWLEDGMENTS

We thank Dr. Gareth Ambler, Biostatistician, Joint UCL/UCLH Biomedical Research Unit, and Dr. Xanthi Pedeli, University of Athens, for their statistical advice. We acknowledge the input of Professor Brian F. Hutton, UCL, regarding image coregistration and ^{18}F-FDG uptake measurements. This study was funded in part by contributions from the Sussex Stroke and Circulation Fund and the Royal College of Radiologists. UCL/UCLH receives a proportion of funding from the Department of Health's NIHR Biomedical Research Centre's funding scheme. No other potential conflict of interest relevant to this article was reported.

REFERENCES

1. Davies MJ. Stability and instability: two faces of coronary atherosclerosis. The Paul Dudley White Lecture 1995. *Circulation.* 1996;94:2013–2020.
2. Sadeghi MM, Glover DK, Lanza GM, Fayad ZA, Johnson LL. Imaging atherosclerosis and vulnerable plaque. *J Nucl Med.* 2010;51(suppl):51S–65S.
3. Rudd JH, Warburton EA, Fryer TD, et al. Imaging atherosclerotic plaque inflammation with [^{18}F]-fluorodeoxyglucose positron emission tomography. *Circulation.* 2002;105:2708–2711.
4. Tawakol A, Migrino RQ, Bashian GG, et al. In vivo ^{18}F-fluorodeoxyglucose positron emission tomography imaging provides a noninvasive measure of carotid plaque inflammation in patients. *J Am Coll Cardiol.* 2006;48:1818–1824.
5. Kerwin W, Hooker A, Spilker M, et al. Quantitative magnetic resonance imaging analysis of neovasculature volume in carotid atherosclerotic plaque. *Circulation.* 2003;107:851–856.
6. Tang TY, Howarth SP, Miller SR, et al. Correlation of carotid atheromatous plaque inflammation using USPIO-enhanced MR imaging with degree of luminal stenosis. *Stroke.* 2008;39:2144–2147.
7. de Weert TT, Ouhlous M, Meijering E, et al. In vivo characterization and quantification of atherosclerotic carotid plaque components with multidetector computed tomography and histopathological correlation. *Arterioscler Thromb Vasc Biol.* 2006;26:2366–2372.
8. Wintermark M, Jawadi SS, Rapp JH, et al. High-resolution CT imaging of carotid artery atherosclerotic plaques. *AJNR.* 2008;29:875–882.
9. Hoffmann U, Moselewski F, Nieman K, et al. Noninvasive assessment of plaque morphology and composition in culprit and stable lesions in acute coronary syndrome and stable lesions in stable angina by multidetector computed tomography. *J Am Coll Cardiol.* 2006;47:1655–1662.
10. Lardinois D, Weder W, Hany TF, et al. Staging of non-small-cell lung cancer with integrated positron-emission tomography and computed tomography. *N Engl J Med.* 2003;348:2500–2507.
11. Groves AM, Speechly-Dick ME, Kayani I, et al. First experience of combined cardiac PET/64-detector CT angiography with invasive angiographic validation. *Eur J Nucl Med Mol Imaging.* 2009;36:2027–2033.
12. Silvera SS, Aidi HE, Rudd JH, et al. Multimodality imaging of atherosclerotic plaque activity and composition using FDG-PET/CT and MRI in carotid and femoral arteries. *Atherosclerosis.* 2009;207:139–143.

13. Kwee RM, Teule GJ, van Oostenbrugge RJ, et al. Multimodality imaging of carotid artery plaques: ^{18}F-fluoro-2-deoxyglucose positron emission tomography, computed tomography, and magnetic resonance imaging. *Stroke.* 2009;40:3718–3724.
14. Rudd JH, Myers KS, Bansilal S, et al. Atherosclerosis inflammation imaging with ^{18}F-FDG PET: carotid, iliac, and femoral uptake reproducibility, quantification methods, and recommendations. *J Nucl Med.* 2008;49:871–878.
15. Liang X, Yang D, Hu J, Hao X, Gao J, Mao Z. Hypoxia inducible factor-alpha expression correlates with vascular endothelial growth factor-C expression and lymphangiogenesis/angiogenesis in oral squamous cell carcinoma. *Anticancer Res.* 2008;28:1659–1666.
16. Motoyama S, Kondo T, Sarai M, et al. Multislice computed tomographic characteristics of coronary lesions in acute coronary syndromes. *J Am Coll Cardiol.* 2007;50:319–326.
17. Ben-Haim S, Kupzov E, Tamir A, Israel O. Evaluation of ^{18}F-FDG uptake and arterial wall calcifications using ^{18}F-FDG PET/CT. *J Nucl Med.* 2004;45:1816–1821.
18. Dunphy MP, Freiman A, Larson SM, Strauss HW. Association of vascular ^{18}F-FDG uptake with vascular calcification. *J Nucl Med.* 2005;46:1278–1284.
19. Menezes LJ, Kayani I, Ben-Haim S, Hutton B, Ell PJ, Groves AM. What is the natural history of ^{18}F-FDG uptake in arterial atheroma on PET/CT? Implications for imaging the vulnerable plaque. *Atherosclerosis.* 2010;211:136–140.
20. Rudd J, Myers K, Bansilal S, et al. The relationships between regional arterial inflammation, calcification, risk factors and biomarkers: a prospective FDG PET/CT imaging study. *Circ: Cardiovasc Imaging.* 2009;2:107–115.
21. Pundziute G, Schuijf JD, Jukema JW, et al. Evaluation of plaque characteristics in acute coronary syndromes: non-invasive assessment with multi-slice computed tomography and invasive evaluation with intravascular ultrasound radiofrequency data analysis. *Eur Heart J.* 2008;29:2373–2381.
22. Muntendam P, McCall C, Sanz J, Falk E, Fuster V, High Risk Plaque Initiative. The BioImage Study: novel approaches to risk assessment in the primary prevention of atherosclerotic cardiovascular disease—study design and objectives. *Am Heart J.* 2010;160:49–57.e1.
23. Graebe M, Pedersen S, Borgwardt L, Højgaard L, Sillesen H, Kjaer A. Molecular pathology in vulnerable carotid plaques: correlation with 18-fluorodeoxyglucose positron emission tomography (FDG-PET). *Eur J Vasc Endovasc Surg.* 2009;37:714–721.
24. Holm PW, Slart RH, Zeebregts CJ, Hillebrands JL, Tio RA. Atherosclerotic plaque development and instability: a dual role for VEGF. *Ann Med.* 2009;41:257–264.
25. Buck A, Reske S. Cellular origin and molecular mechanisms of ^{18}F-FDG uptake: is there a contribution of the endothelium? *J Nucl Med.* 2004;45:461–463.
26. Menezes LJ, Kotze CW, Hutton BF, et al. Vascular inflammation imaging with ^{18}F-FDG PET/CT: when to image? *J Nucl Med.* 2009;50:854–857.
27. Tahara N, Kai H, Ishibashi M, et al. Simvastatin attenuates plaque inflammation: evaluation by fluorodeoxyglucose positron emission tomography. *J Am Coll Cardiol.* 2006;48:1825–1831.
28. Izquierdo-Garcia D, Davies JR, Graves MJ, et al. Comparison of methods for magnetic resonance-guided [18-F]fluorodeoxyglucose positron emission tomography in human carotid arteries: reproducibility, partial volume correction, and correlation between methods. *Stroke.* 2009;40:86–93.
29. Papathanasiou ND, Du Y, Menezes LJ, et al. 18F-Fluorodeoxyglucose PET/CT in the evaluation of large-vessel vasculitis: diagnostic performance and correlation with clinical and laboratory parameters. *British J Radiol.* March 8, 2011 [Epub ahead of print].
30. Goldstein JA, Demetriou D, Grines CL, Pica M, Shoukfeh M, O'Neill WW. Multiple complex coronary plaques in patients with acute myocardial infarction. *N Engl J Med.* 2000;343:915–922.
31. Bitar R, Moody AR, Leung G, et al. In vivo 3D high-spatial-resolution MR imaging of intraplaque hemorrhage. *Radiology.* 2008;249:259–267.